

Journal of Materials Chemistry A

Accepted Manuscript



This is an *Accepted Manuscript*, which has been through the Royal Society of Chemistry peer review process and has been accepted for publication.

Accepted Manuscripts are published online shortly after acceptance, before technical editing, formatting and proof reading. Using this free service, authors can make their results available to the community, in citable form, before we publish the edited article. We will replace this *Accepted Manuscript* with the edited and formatted *Advance Article* as soon as it is available.

You can find more information about *Accepted Manuscripts* in the [Information for Authors](#).

Please note that technical editing may introduce minor changes to the text and/or graphics, which may alter content. The journal's standard [Terms & Conditions](#) and the [Ethical guidelines](#) still apply. In no event shall the Royal Society of Chemistry be held responsible for any errors or omissions in this *Accepted Manuscript* or any consequences arising from the use of any information it contains.

COMMUNICATION

Black Titanium Oxide Nanoarray Electrodes for High Rate Li-ion Microbatteries

Cite this: DOI: 10.1039/x0xx00000x

Ji-Yong Eom,^a Sung-Jin Lim,^b Sang-Min Lee,^c Won-Hee Ryu,^{d,*} and Hyuk-Sang Kwon,^{b,*}

Received 00th January 2012,
Accepted 00th January 2012

DOI: 10.1039/x0xx00000x

www.rsc.org/

Black TiO_{2-x} nanotube arrays, which are synthesized by an electrochemical method and subsequent thermal conversion in a hydrogen atmosphere, are employed as a binder-free, free-standing electrode for high rate Li-ion microbatteries. Excellent cyclability and superior rate capability are achieved by an oxygen-deficient structure of TiO₂ with increased electronic conductivity and the formation of metallic titanium hydride phases on the substrate.

The micro energy storage system has emerged as a focal point of future energy devices in line with the miniaturization of high performance electronic devices¹⁻³. The development of ultrathin electrodes of submicron scale is essentially required for the realization of micro-sized batteries⁴. Building up tailored electrode architectures arranged at nanoscale order has recently been considered to maximize the performance of microbatteries owing to the limited loading space for active materials on the thin electrode substrate⁵⁻⁸. As a function of their numerable reaction sites, electrodes with high surface area can ensure superb kinetic properties and improved capacity for operation, consequently affording high power and energy density⁹⁻¹². Titanium oxide (TiO₂) nanotubes have attracted much attention as a prospective electrode system for microbatteries due to their advantageous material properties and facile fabrication process¹³⁻¹⁵. Compared to other types of anode materials such as carbonaceous materials and Li-M alloys (M=Si, Sn), TiO₂ offers beneficial aspects originating from enhanced safety, good cycling and non-toxicity¹⁶⁻¹⁸. TiO₂ nanotubes have been grown directly on Ti substrate via electrochemical methodology as a binder-free electrode, and their unique features with vertically aligned nanopores can improve rate performance resulting from the extensive electrochemical surfaces and short diffusion length for Li⁺ through the nanotube walls^{19, 20}. In previous studies, subsequent heat treatment of as-prepared TiO₂ nanotubes was

conducted to reinforce the adhesion strength between the TiO₂ nanotubes and Ti substrate. However, the crystalline anatase phases of the TiO₂ nanotubes obtained by post-thermal treatment at approximately 400 °C often suffer from (i) slow electron transfer originating from a huge band gap (~ 3.3 eV value)²¹ and (ii) the local structural distortion caused by a phase transition that occurs during the insertion and extraction of Li⁺¹³. Moreover, a passive oxidation layer on the Ti substrate accompanying heat treatment under air atmosphere hinders the fast electron transfer from the substrate to the TiO₂ anode and deteriorates the kinetic performance at high current rates.

Recently, it was reported that a highly conductive TiO₂ nanostructure called 'black TiO₂' is more attractive for photovoltaics and photocatalysis owing to its narrower bandgap of approximately 2.2 eV and consequent high electrical conductivity²¹⁻²⁵. Black TiO₂ is simply prepared via thermal treatment in a hydrogen atmosphere, and the oxidation number of Ti ions in TiO₂ phase is partially reduced. The donor density of reduced TiO₂ nanostructures proportional to electrical conductivity is significantly improved by the formation of oxygen vacancy/Ti³⁺ sites²⁶, and hydroxyl groups tend to form on the oxygen-deficient, disordered surface of TiO_{2-x} nanostructures during hydrogenation, which could modify the electronic properties and electrochemical activity of the TiO₂ nanostructures^{25, 27, 28}. Moreover, the electrical conductivity of the Ti substrate could be effectively preserved without unwanted oxidation of the substrate by calcination under a reducing atmosphere. The functional conversion treatment of the TiO₂ nanoarray phase should be adapted to effectively yield a high-power-capable thin-film battery cell suitable for micro-device applications.

In this communication, we introduce highly conductive black TiO_{2-x} nanotube arrays (NTs) as binder-free ultrathin electrodes

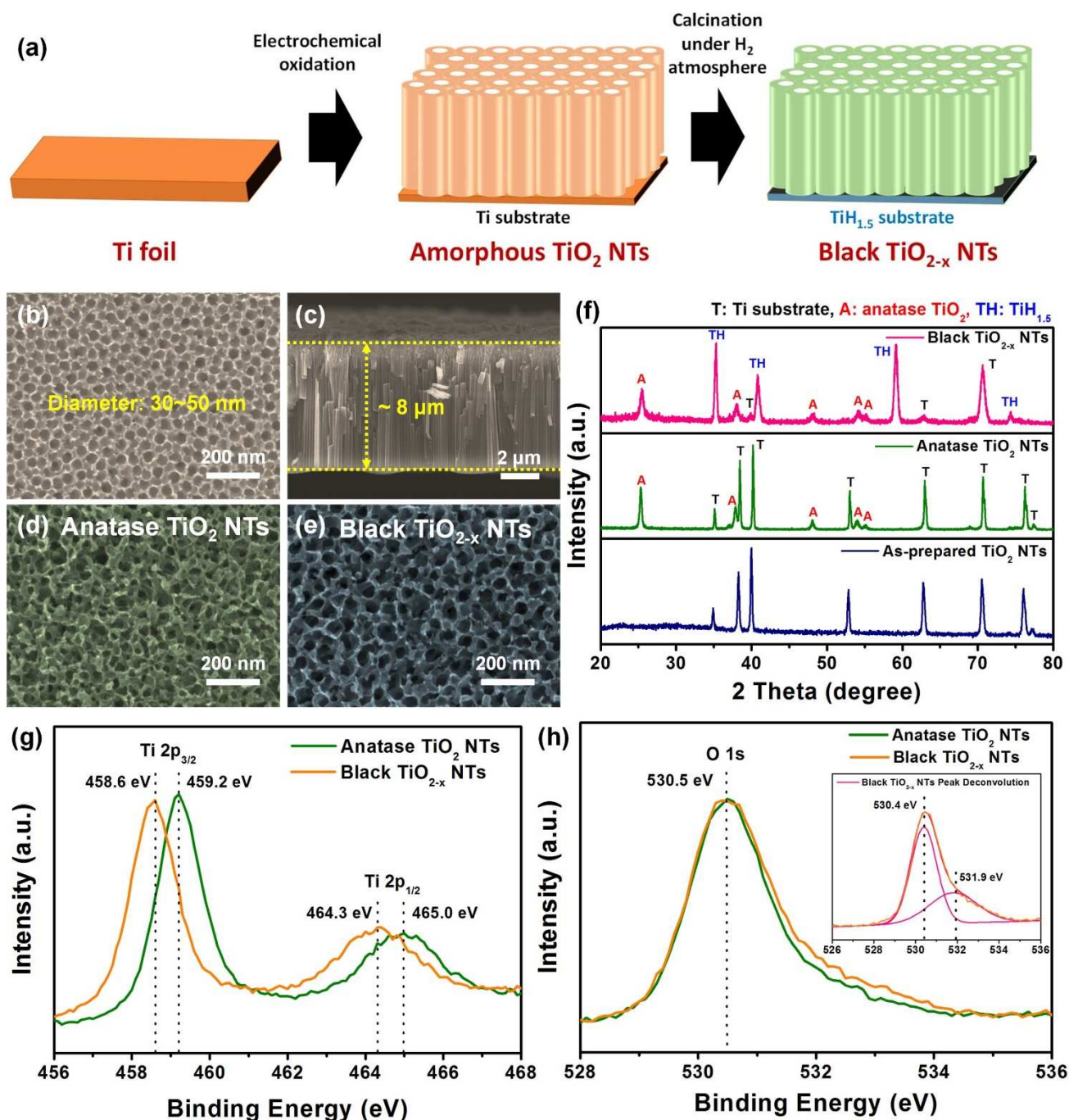


Fig. 1 (a) Schematic illustration of the synthetic strategy for a black TiO_{2-x} NT electrode; (b) surface and (c) cross-sectional morphology of the as-prepared TiO_2 NTs; surface morphology of the (d) anatase TiO_2 NTs and (e) black TiO_{2-x} NTs; (f) X-ray diffraction patterns of as-prepared TiO_2 NTs, anatase TiO_2 NTs, and black TiO_{2-x} NTs (JCPDS No. 21-1272 for TiO_2 , JCPDS No. 65-3362 for Ti, JCPDS No. 78-2216 for $\text{TiH}_{1.5}$); X-ray photoelectron spectra obtained from black TiO_{2-x} NTs collected in the (g) Ti 2p and (h) O 1s regions. The inset figure is the O 1s peak of the black TiO_{2-x} NTs deconvoluted into two peaks centered at ~ 530.4 and ~ 531.9 eV.

for high rate Li-ion microbatteries. The black TiO_{2-x} NTs were easily prepared by simple electrochemical methodology and subsequent thermal conversion under hydrogen atmosphere (Fig. 1a). The modified TiO_{2-x} nanostructure with a high concentration of oxygen vacancies can offer improved electron conductivity and facile Li^+ ion diffusion in the structure. The morphological features and crystalline phase of the black TiO_{2-x}

NT electrodes were investigated. The electrochemical properties of the black TiO_{2-x} NT electrodes were examined to evaluate any advantages from the modified phase structure compared with anatase TiO_2 NT (white TiO_2 NT) electrodes prepared by thermal treatment in air. We also report the formation of metallic titanium hydride on Ti substrate,

preserving electron transport without unwanted passivation layer formation on the substrate.

Smooth and well-ordered TiO₂ NTs were successfully grown on a Ti disk by simple electrochemical oxidation in a non-aqueous solution containing fluoride ions as reported in our previous work and as shown in Fig. 1b and 1c¹³. The diameter of the as-prepared TiO₂ NTs was approximately 30~50 nm (Fig. 1b) with a wall thickness of approximately 5~10 nm and an average tube length of ~ 8 μm (Fig. 1c). To obtain black TiO₂ NTs and anatase TiO₂ NTs, the as-prepared TiO₂ nanotubes were annealed at 450 °C for 2 h in a hydrogen atmosphere or in air, respectively. Figs. 1d and 1e present the surface morphology of the anatase TiO₂ nanotubes and the black TiO₂ nanotubes. Crystalline particle growth at the pores and walls of both TiO₂ nanotube samples was observed slightly after annealing at 450 °C, and the surface morphology of both TiO₂ nanotube samples was crumbled partially after annealing. It has been previously reported that a structural transformation and subsequent crystal growth of TiO₂ occur during thermal treatment above 400 °C^{29,30}. The crystalline phase information of the TiO₂ NTs was examined by obtaining XRD patterns of the samples (Fig. 1f). For the as-prepared TiO₂ NTs, typical Ti peaks were observed, indicating that the as-prepared TiO₂ NTs obtained by the electrochemical oxidation method form an amorphous structure. After the subsequent thermal treatment, calcination of the TiO₂ NTs in either of the different atmospheres led to the crystallization of the anatase phase. Although the peak position of the anatase phase in both samples corresponded well, the peak width of the black TiO₂ NTs was wider than that of the anatase TiO₂ NTs for all peaks. This result demonstrates that the crystallization of the black TiO₂ NTs to uniform anatase phase was prevented by the hydrogen atmosphere. Ti⁴⁺ ions in the TiO₂ phase were reduced by heating under the hydrogen environment, and the TiO₂ structure tended to form an oxygen-deficient TiO_{2-x} phase (black TiO₂ phase) with low crystallinity. Moreover, titanium hydride (TiH_{1.5}) peaks for the black TiO_{2-x} NT samples appeared, indicating that the Ti substrate was transformed to TiH_{1.5}. It has been previously reported that Ti is known to absorb large quantities of hydrogen, and this hydrogenation transforms the Ti from metal (hcp A3, α-phase) to hydride (TiH_{2-x} (x < 0.5), fcc C1, δ-phase)³¹⁻³³. Thus, TiH_{1.5} can exist as an α+δ biphasic material. Ito et al. reported that the electrical conductivity of TiH_{1.53} (1.32 × 10⁶ Ω⁻¹ m⁻¹) at 323K approaches that of Ti metal (1.59 × 10⁶ Ω⁻¹ m⁻¹)³². The Ti substrate surface is easily oxidized after calcination of as-prepared TiO₂ NT samples in air, and consequently the passive oxidation layer on the surface often impedes the electron movement transferring from/to external wires and the power supply. On the other hand, the formation of TiH_{1.5} phases on Ti substrate enables it to provide a fast electron pathway to black TiO_{2-x} anodes without a passivation barrier.

The surface characterization of the TiO₂ NTs obtained in different atmospheres was carried out to further examine the effect of hydrogenation on their chemical composition and oxidation state (Fig. 1g and 1h). The Ti 2p core level XPS

spectra of the anatase and black TiO_{2-x} NTs had two broad peaks corresponding to the characteristic Ti 2p_{3/2} and Ti 2p_{1/2} peaks, as presented in Fig. 1g. In the case of the anatase TiO₂ NTs, Ti 2p_{3/2} and Ti 2p_{1/2} peaks centered at ~459.2 and ~465.0 eV were observed, and these two peaks correspond to the Ti 2p_{3/2} and Ti 2p_{1/2} peaks of Ti⁴⁺ in TiO₂^{24,34}. On the other hand, a negative shift of these two peaks for the black TiO_{2-x} NTs was found in the binding energy, demonstrating different bonding environments. These two peaks centered at ~458.6 and ~464.3 eV, corresponding to the Ti 2p_{3/2} and Ti 2p_{1/2} peaks of Ti³⁺, confirmed the creation of room-temperature stable isolated Ti³⁺ defect-structure in the anatase^{24,27}. This result suggests that oxygen vacancies were created in the bulk TiO_{2-x} NTs by annealing in a hydrogen atmosphere. The high oxygen deficiencies in TiO_{2-x} would be formed either by removal of oxygen from the anion sublattice leaving oxygen vacancies, or by formation of Ti interstitials, but oxygen vacancies are most likely more predominant defects than Ti interstitials in the generality of cases³⁵⁻³⁷. The formation of oxygen vacancies contributes to an increase in density of carriers, which are known to be the electron donors for TiO₂ nanostructures. The higher donor density in the TiO_{2-x} structure led to an increase in the electrical conductivity and a decrease in the bandgap energy, consequently affording excellent kinetic properties to Li-ion cells employing the black TiO_{2-x} NT electrodes. No Ti²⁺ peak related to titanium hydride phases (TiH_{2-x}, x ≤ 0.5) was observed in the Ti 2p XPS spectra, verifying that the TiH_{1.5} phase was only formed at the Ti substrate^{34,38}. The O 1s core level XPS spectra of the anatase TiO₂ NTs and black TiO_{2-x} NTs are shown in Fig. 1h. Both samples exhibited a peak of ~530.5 eV corresponding to the characteristic peak of Ti-O-Ti^{22,36,37}. In the O 1s peak of the black TiO_{2-x} NTs, not only a broader peak centered at ~530.5 eV but also an additional shoulder at higher binding energy was observed compared with the anatase TiO₂ NTs. This broad peak could be deconvoluted into two peaks centered at ~530.4 and ~531.9 eV (inset of Fig. 1h). The peak of ~531.9 eV is attributed to Ti-OH bonding located at the binding energy of ~1.5~1.8 eV³⁹. Defective oxygen sites on the surface of the black TiO_{2-x} NTs, caused by the reducing environment during thermal treatment, could tend to bind with hydrogens and then locally form hydroxyl surface groups.

The charge-discharge profiles of the black TiO_{2-x} NTs and anatase TiO₂ NTs were compared to investigate the reaction mechanism for Li insertion/extraction. Fig. 2 presents the charge-discharge curves in the 1st, 2nd, and 3rd cycles for the anatase TiO₂ NTs and black TiO_{2-x} NTs between 1.0 and 3.0 V at a current density of 0.1 mA cm⁻². Voltage plateaus at ~1.7 and ~2.0 V were observed in the charge-discharge curves of both anatase TiO₂ NTs and black TiO_{2-x} NTs, which can be attributed to the insertion and extraction of Li⁺ through tetrahedral and octahedral sites of the crystalline anatase phase, respectively¹⁵. The anatase TiO₂ phase starts to react with Li⁺ ions at the surface facing the electrolyte, and then the TiO₂ phase is transformed into a Li_{0.5}TiO₂ phase. The interface between the outer Li_{0.5}TiO₂/inner TiO₂ migrates (two-phase

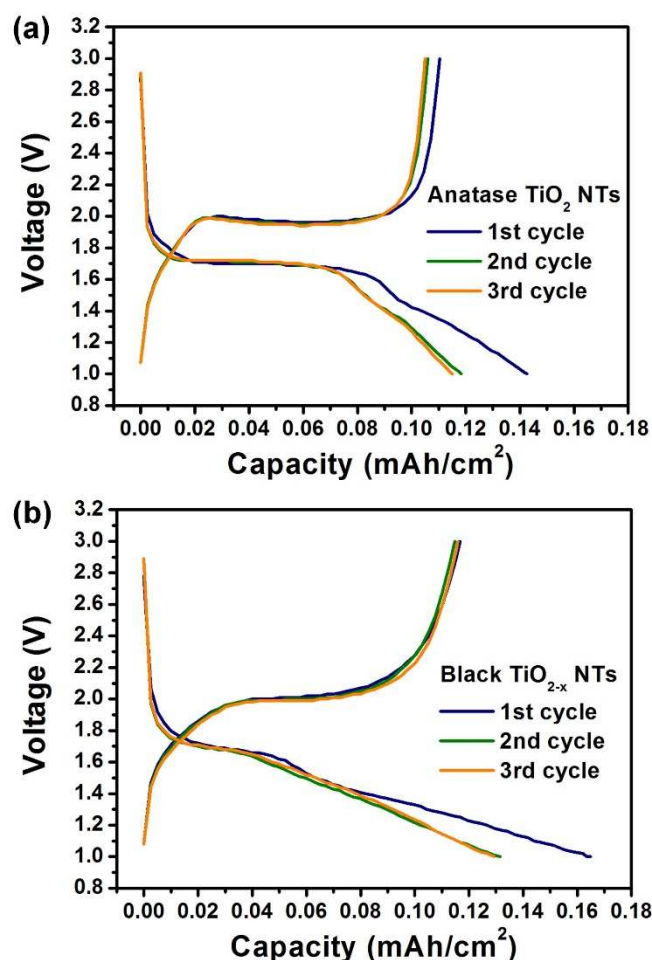


Fig. 2 Initial charge-discharge profiles in the 1st, 2nd, and 3rd cycles for the (a) anatase TiO_2 NT electrode and (b) black TiO_{2-x} NT electrode. The electrochemical experiments were performed over a voltage window between 1.0 and 3.0 V at a current density of 0.1 mA cm^{-2} .

reaction) along the inner direction and consequently $\text{Li}_{0.5}\text{TiO}_2$ exists in the structure. Whereas the Li-insertion/extraction reaction of anatase TiO_2 NTs occurred only via a two-phase reaction, the charge-discharge curve of the black TiO_{2-x} NTs becomes similar to a mixture of the shapes of the anatase TiO_2 and amorphous TiO_2 NT curves. We previously reported a sloping curve characteristic of amorphous TiO_2 NTs (as-prepared TiO_2 NTs) without a plateau. The insertion and extraction of Li^+ in the amorphous TiO_2 nanotubes occurs homogeneously without a two-phase reaction between Li_xTiO_2 and TiO_2 ($x\text{Li}^+ + xe^- + \text{TiO}_2 \leftrightarrow \text{Li}_x\text{TiO}_2$, $0.5 < x < 1$)^{13, 40}. Therefore, the charge-discharge curve characteristics of black TiO_{2-x} NTs support the idea that the amorphous phase remains without transforming into the anatase phase after thermal conversion treatment in a hydrogen atmosphere. The initial charge and discharge capacities of the black TiO_{2-x} NTs (0.165 and $0.117 \text{ mAh cm}^{-2}$) were higher than those of the anatase TiO_2 NTs (0.143 and $0.110 \text{ mAh cm}^{-2}$), indicating that the black TiO_{2-x} NTs would be available to accommodate more Li^+ per TiO_2 compared with the anatase TiO_2 NTs due to the co-existence of an amorphous TiO_2 phase. A slightly higher

irreversible capacity was also found for the black TiO_{2-x} NTs (29 % of 1st charge capacity) compared to the A- TiO_2 NTs (23 % of 1st charge capacity) because there were structural and chemical defects acting as Li^+ traps in the amorphous phase of the black TiO_{2-x} NTs.¹³

To confirm the superb kinetic properties of black TiO_{2-x} NTs, a rate capability test was conducted between 1.0 and 3.0 V at various current densities (Fig. 3a). To fully activate the nanotube electrode during the initial cycles, the rate capability tests were performed after the 10th cycle at a current density of 0.1 mA cm^{-2} . The discharge capacities of the anatase TiO_2 NTs and black TiO_{2-x} NTs at low current density (0.1 mA cm^{-2}) were similar to each other. However, as the current density increased, the discharge capacity of the black TiO_{2-x} NTs was obviously higher than that of the anatase TiO_2 NTs. At the high current density of 10 mA cm^{-2} , the discharge capacities of the anatase TiO_2 NTs and black TiO_{2-x} NTs maintained nearly 44 and 72 % of their discharge capacity at the current density of 0.1 mA cm^{-2} , respectively. This result suggests that the rate performance of the cell was significantly improved by the introduction of black TiO_{2-x} NTs due to the improved electrical conductivity of the TiO_2 structure and the facile reaction with Li^+ ions via the amorphous phase. The improved kinetic properties of the black TiO_{2-x} NTs were assessed by EIS measurements and compared with those of the anatase TiO_2 NTs (Fig. 3b). Two separated semicircles in the high and intermediate frequency range of 100–0.01 kHz and a sloping line in the low frequency range of 10–0.01 Hz were observed in the Nyquist plots of EIS for the anatase TiO_2 NTs and black TiO_{2-x} NTs at fully charged state after the 10th cycle at a current density of 0.1 mA cm^{-2} . In the equivalent circuit, R_b is the bulk resistance of the electrolyte, separator, and Li anode at high frequency with resistance loss from the first semicircle; $CPE1$ and R_{SEI} are the capacitance and the resistance, respectively, of the solid-state interface layer formed as a passivation layer after full charge of the electrode, related to the first semicircle at high frequency; $CPE2$ and R_{ct} are the double layer capacitance and the charge transfer resistance, respectively, related to the second semicircle at intermediate frequency; and W is the Warburg impedance, which corresponds to a sloping line at the low frequency indicating Li ion diffusion in the electrode^{41, 42}. Almost identical shape and resistance values were observed for the first semicircle (R_b , $CPE1$, and R_{SEI}) between the two electrodes, verifying the uniformity of the cell tests. The charge transfer resistance (R_{ct}) of the black TiO_{2-x} NTs (47Ω) at the intermediate frequency was much smaller than that of the anatase TiO_2 NTs (72Ω). The black TiO_{2-x} NTs can offer relatively high electron conductivity due to high donor density originating from oxygen vacancy in the TiO_{2-x} structure.

Improved cycling properties of the black TiO_{2-x} NTs under different current rates were also demonstrated compared with those of the anatase TiO_2 NTs (Figs. 3c and 3d). Herein, the current density of 1 mA cm^{-2} corresponds to that of ~ 10 C-rate because the discharge capacity of both samples is approximately 0.1 mAh cm^{-2} at low current density (Fig. 2). At low current density of 0.1 mA cm^{-2} , the anatase TiO_2 NTs and

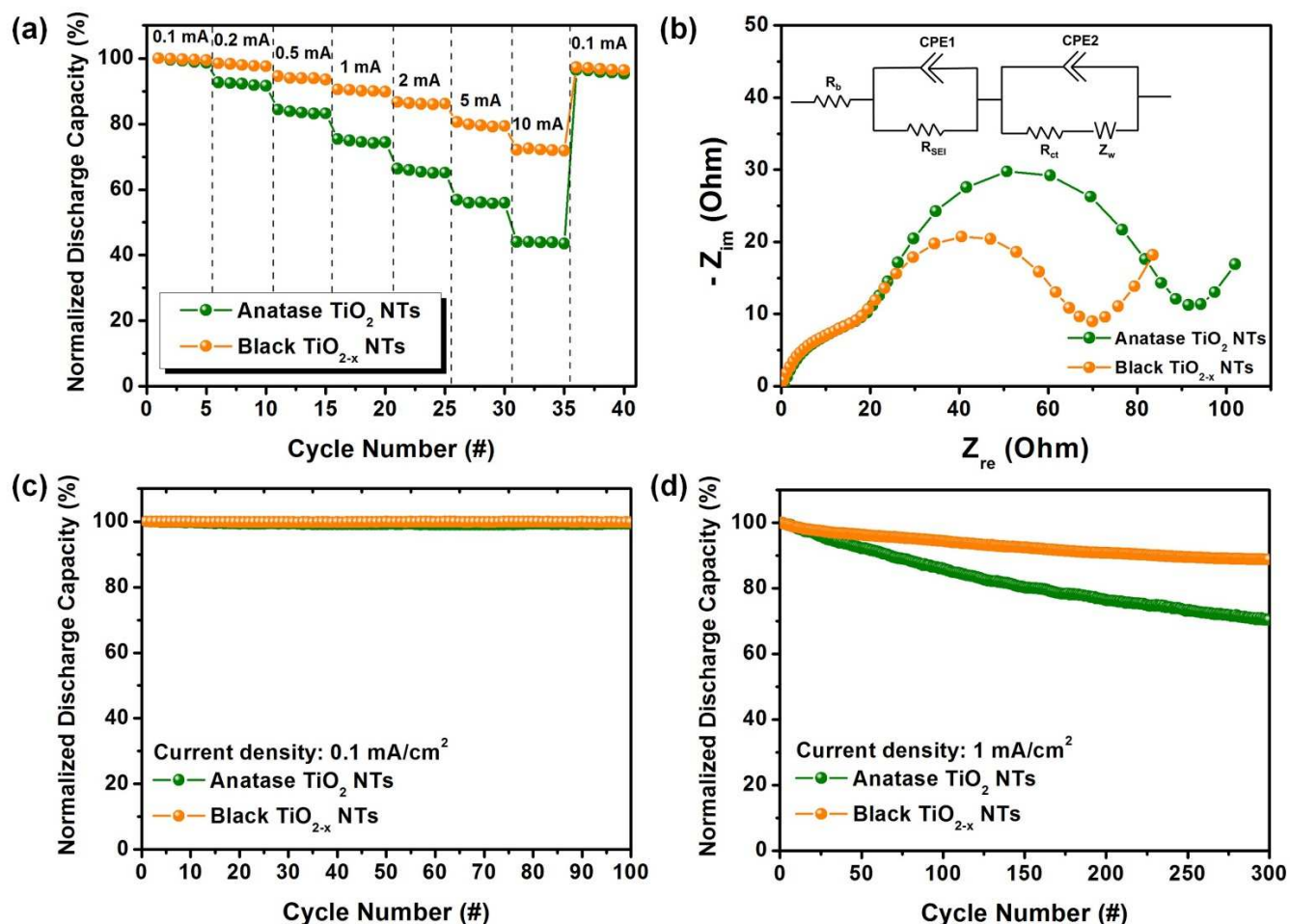


Fig. 3 (a) Rate capabilities during cycling of the anatase TiO₂ NT and black TiO_{2-x} NT electrodes at various current densities. The samples were cycled at a current density of 0.1 mA cm⁻² for 10 cycles and then were cycled 5 times at each current density. (b) Electrochemical impedance spectroscopy (EIS) spectra of the anatase TiO₂ NT and black TiO_{2-x} NT electrodes. The inset figure presents the corresponding equivalent circuit, in which R_b , R_{SEI} , $CPE1$, R_{ct} , $CPE2$, and Z_w represent the bulk resistance; resistance and capacitance of the solid-state interface layer; double layer capacitance and charge transfer resistance of the electrodes; and Warburg impedance, respectively. Cycling performance (expressed by normalized capacities) of the A-TiO₂ NTs and H-TiO₂ NTs at a current density of (c) 0.1 mA cm⁻² for 100 cycles, and (d) at 1 mA cm⁻² for 300 cycles. The cycle data were collected after 10 cycles. All electrochemical cycling experiments were performed over a voltage window between 1.0 and 3.0 V.

black TiO_{2-x} NTs showed very stable and similar cycling with capacity retention of ~99 % after 100 cycles (Fig. 3c). On the other hand, at the 100-fold higher current density of 1 mA cm⁻², the black TiO_{2-x} NTs (89 %) exhibited much higher capacity retention than the anatase TiO₂ NTs (70 %) compared with their initial discharge capacity after 300 cycles (Fig. 3d). This result indicates that the ultrafast insertion and extraction of Li⁺ through the black TiO_{2-x} NTs has been successfully achieved. The black TiO_{2-x} NTs hint at the development of high rate TiO₂ thin-film electrodes for the realization of high performance microbatteries.

Conclusions

In summary, we synthesized black TiO_{2-x} NTs through thermal conversion treatment of amorphous TiO₂ NTs under hydrogen atmosphere and succeeded in obtaining excellent electrochemical performance and kinetic properties from black TiO_{2-x} NT electrodes for high rate Li-ion microbatteries. After

the thermal conversion under hydrogen, the black TiO_{2-x} NT electrodes generated reduced Ti³⁺ ions with oxygen vacancies in the structure, which improve the electronic conductivity of TiO₂ structure by increasing its carrier density. Moreover, the partial Ti substrate turned into a metallic TiH_{1.5} phase instead of forming an anatase TiO₂ passive layer on the substrate, which is easily formed after heat treatment in air. The charge-discharge curves of the black TiO_{2-x} NT electrode show different reaction characteristics mixed between amorphous (1-phase reaction) and anatase (2-phase reaction) phase, whereas those of the anatase TiO₂ NT electrode only show a 2-phase reaction. The black TiO_{2-x} NT electrode delivered stable cycling performance for 300 cycles at a high current rate of 1 mA cm⁻² (~10 C) and showed excellent rate capability even at 10 mA cm⁻² (~100 C) compared to an anatase TiO₂ NT electrode owing to its improved electronic features and kinetic properties. Our synthetic strategy for the creation of a black TiO_{2-x} NT

electrode can be extended to other possible TiO₂ anodes in an effort to improve the performance of microbatteries.

Acknowledgements

This work was funded by POSCO steel and the BK21 Program of the Korea Ministry of Knowledge Economy. This work (Grants No. C0199439) was also supported by Business for Cooperative R&D between Industry, Academy, and Research Institute funded Korea Small and Medium Business Administration in 2014.

Notes and references

^a Clean & Energy Materials R&D Center, Korea Automotive Technology Institute, Cheonan, Chungnam 330-912, Republic of Korea

^b Department of Materials Science and Engineering, Korea Advanced Institute of Science and Technology, Daejeon 305-701, Republic of Korea.; E-mail: hskwon@kaist.ac.kr (Hyuk-Sang Kwon)

^c Battery Research Center, Korea Electrotechnology Research Institute, Changwon, Gyeongnam 642-120, Republic of Korea

^d Department of Chemical and Environmental Engineering, Yale University, New Haven, Connecticut 06520-8286, United States.; E-mail: wonhee.ryu@yale.edu (Won-Hee Ryu)

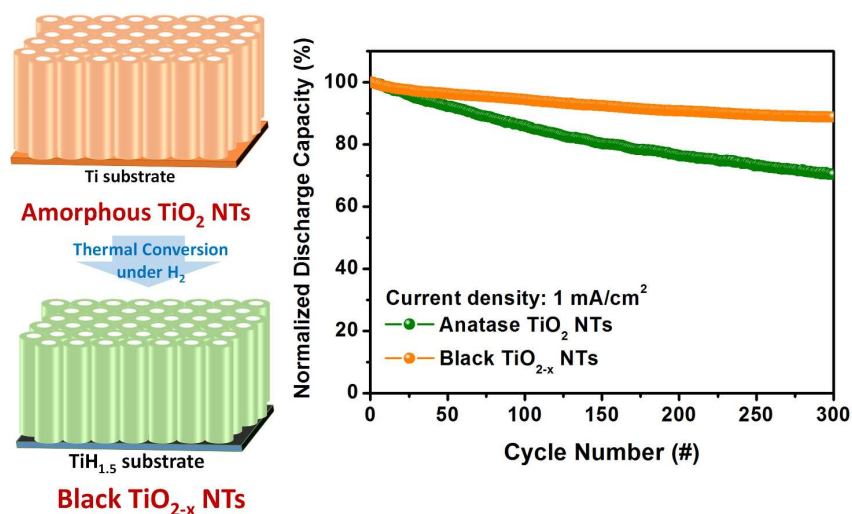
† Electronic Supplementary Information (ESI) available: [Experimental procedure]. See DOI: 10.1039/c000000x/

- P. V. Braun and R. G. Nuzzo, *Nat Nanotechnol*, 2014, **9**, 962-963.
- M. Armand and J. M. Tarascon, *Nature*, 2008, **451**, 652-657.
- R. R. Salunkhe, Y. H. Lee, K. H. Chang, J. M. Li, P. Simon, J. Tang, N. L. Torad, C. C. Hu and Y. Yamauchi, *Chem-Eur J*, 2014, **20**, 13838-13852.
- C. Y. Liu, E. I. Gillette, X. Y. Chen, A. J. Pearse, A. C. Kozen, M. A. Schroeder, K. E. Gregorczyk, S. B. Lee and G. W. Rubloff, *Nat Nanotechnol*, 2014, **9**, 1031-1039.
- J. Ren, L. Li, C. Chen, X. L. Chen, Z. B. Cai, L. B. Qiu, Y. G. Wang, X. R. Zhu and H. S. Peng, *Adv Mater*, 2013, **25**, 1155-1159.
- J. L. Liu, W. W. Zhou, L. F. Lai, H. P. Yang, S. H. Lim, Y. D. Zhen, T. Yu, Z. X. Shen and J. Y. Lin, *Nano Energy*, 2013, **2**, 726-732.
- J. H. Choi, W. H. Ryu, K. Park, J. D. Jo, S. M. Jo, D. S. Lim and I. D. Kim, *Sci Rep-Uk*, 2014, **4**.
- J. Ye, A. C. Baumgaertel, Y. M. Wang, J. Biener and M. M. Biener, *ACS Nano*, 2014.
- M. Wagemaker and F. M. Mulder, *Accounts Chem Res*, 2013, **46**, 1206-1215.
- Y. K. Sun, Z. H. Chen, H. J. Noh, D. J. Lee, H. G. Jung, Y. Ren, S. Wang, C. S. Yoon, S. T. Myung and K. Amine, *Nature Mater*, 2012, **11**, 942-947.
- K. T. Lee and J. Cho, *Nano Today*, 2011, **6**, 28-41.
- W. H. Ryu, J. W. Jung, K. Park, S. J. Kim and I. D. Kim, *Nanoscale*, 2014, **6**, 10975-10981.
- W. H. Ryu, D. H. Nam, Y. S. Ko, R. H. Kim and H. S. Kwon, *Electrochim Acta*, 2012, **61**, 19-24.
- N. A. Kyeremateng, N. Plylahan, A. C. S. dos Santos, L. V. Taveira, L. F. P. Dick and T. Djenizian, *Chem Commun*, 2013, **49**, 4205-4207.
- G. F. Ortiz, I. Hanzu, T. Djenizian, P. Lavela, J. L. Tirado and P. Knauth, *Chem Mater*, 2009, **21**, 63-67.
- Y. Ren, Z. Liu, F. Pourpoint, A. R. Armstrong, C. P. Grey and P. G. Bruce, *Angew Chem Int Edit*, 2012, **51**, 2164-2167.
- D. Deng, M. G. Kim, J. Y. Lee and J. Cho, *Energ Environ Sci*, 2009, **2**, 818-837.
- G. N. Zhu, Y. G. Wang and Y. Y. Xia, *Energ Environ Sci*, 2012, **5**, 6652-6667.
- A. Lamberti, N. Garino, A. Sacco, S. Bianco, A. Chiodoni and C. Gerbaldi, *Electrochim Acta*, 2015, **151**, 222-229.
- K. Y. Xie, M. Guo, W. Lu and H. T. Huang, *Nanotechnology*, 2014, **25**.
- A. Naldoni, M. Allieta, S. Santangelo, M. Marelli, F. Fabbri, S. Cappelli, C. L. Bianchi, R. Psaro and V. Dal Santo, *J Am Chem Soc*, 2012, **134**, 7600-7603.
- X. B. Chen, L. Liu, P. Y. Yu and S. S. Mao, *Science*, 2011, **331**, 746-750.
- N. Liu, C. Schneider, D. Freitag, M. Hartmann, U. Venkatesan, J. Muller, E. Spiecker and P. Schmuki, *Nano Lett*, 2014, **14**, 3309-3313.
- H. L. Cui, W. Zhao, C. Y. Yang, H. Yin, T. Q. Lin, Y. F. Shan, Y. Xie, H. Gu and F. Q. Huang, *J Mater Chem A*, 2014, **2**, 8612-8616.
- Y. H. Hu, *Angewandte Chemie*, 2012, **51**, 12410-12412.
- M. K. Nowotny, T. Bak and J. Nowotny, *J Phys Chem B*, 2006, **110**, 16270-16282.
- X. B. Chen, L. Liu, Z. Liu, M. A. Marcus, W. C. Wang, N. A. Oyler, M. E. Grass, B. H. Mao, P. A. Glans, P. Y. Yu, J. H. Guo and S. S. Mao, *Sci Rep-Uk*, 2013, **3**.
- J. Y. Shin, J. H. Joo, D. Samuelis and J. Maier, *Chem Mater*, 2012, **24**, 543-551.
- B. Erjavec, R. Dominko, P. Umek, S. Sturm, S. Pejovnik, M. Gaberscek and J. Jamnik, *Electrochem Commun*, 2008, **10**, 926-929.
- B. Vijayan, N. M. Dimitrijevic, T. Rajh and K. Gray, *J Phys Chem C*, 2010, **114**, 12994-13002.
- D. Setoyama, J. Matsunaga, H. Muta, M. Uno and S. Yamanaka, *J Alloy Comp*, 2004, **381**, 215-220.
- M. Ito, D. Setoyama, J. Matsunaga, H. Muta, K. Kurosaki, M. Uno and S. Yamanaka, *J Alloy Comp*, 2006, **420**, 25-28.
- Y. Liu, W. Xiang, G. L. Zhang and B. Y. Wang, *Appl Surf Sci*, 2013, **285**, 557-563.
- W. H. Ryu, Y. W. Lee, Y. S. Nam, D. Y. Youn, C. B. Park and I. D. Kim, *J Mater Chem A*, 2014, **2**, 5610-5615.
- D. W. Liu, Y. H. Zhang, P. Xiao, B. B. Garcia, Q. F. Zhang, X. Y. Zhou, Y. H. Jeong and G. Z. Cao, *Electrochim Acta*, 2009, **54**, 6816-6820.
- G. M. Wang, H. Y. Wang, Y. C. Ling, Y. C. Tang, X. Y. Yang, R. C. Fitzmorris, C. C. Wang, J. Z. Zhang and Y. Li, *Nano Lett*, 2011, **11**, 3026-3033.
- X. H. Lu, G. M. Wang, T. Zhai, M. H. Yu, J. Y. Gan, Y. X. Tong and Y. Li, *Nano Lett*, 2012, **12**, 1690-1696.
- W. Lisowski, A. H. J. van den Berg, D. Leonard and H. J. Mathieu, *Surf Interface Anal*, 2000, **29**, 292-297.
- E. McCafferty and J. P. Wightman, *Surf Interface Anal*, 1998, **26**, 549-564.
- Q. Gao, M. Gu, A. M. Nie, F. Mashayek, C. M. Wang, G. M. Odegard and R. Shahbazian-Yassar, *Chem Mater*, 2014, **26**, 1660-1669.
- B. L. He, B. Dong and H. L. Li, *Electrochem Commun*, 2007, **9**, 425-430.
- J. Wang, Y. K. Zhou, Y. Y. Hu, R. O'Hayre and Z. P. Shao, *J Phys Chem C*, 2011, **115**, 2529-2536.

A table of contents (TOC)

Journal of Materials Chemistry A

“ Black Titanium Oxide Nanoarray Electrodes for High Rate Li-ion Microbatteries ”



Black TiO_{2-x} nanotube arrays, which are synthesized by an electrochemical method and subsequent thermal conversion in a hydrogen atmosphere, are employed as a binder-free, free-standing electrode for high rate Li-ion microbatteries. Excellent cyclability and superior rate capability are achieved by an oxygen-deficient structure of TiO₂ with increased electronic conductivity and the formation of metallic titanium hydride phases on the substrate.